Enhanced fluorescence emission from quantum dots on a photonic crystal surface

NIKHIL GANESH[1,2], **WEI ZHANG**[1,2], **PATRICK C. MATHIAS**[1], **EDMOND CHOW**[3], **J. A. N. T. SOARES**[4], **VIKTOR MALYARCHUK**[2], **ADAM D. SMITH**[5] **AND BRIAN T. CUNNINGHAM**[1]*

[1]Nano Sensors Group, University of Illinois at Urbana-Champaign, 208 North Wright Street, Urbana, Illinois 61801, USA
[2]Department of Materials Science and Engineering, University of Illinois at Urbana-Champaign, 1304 West Green Street, Urbana, Illinois 61801, USA
[3]Micro and Nanotechnology Laboratory, University of Illinois at Urbana-Champaign, 208 North Wright Street, Urbana, Illinois 61801, USA
[4]Frederick Seitz Materials Research Laboratory, University of Illinois at Urbana-Champaign, 104 South Goodwin Avenue, Urbana, Illinois 61801, USA
[5]Department of Physics, University of Illinois at Urbana-Champaign 1110 West Green Street, Urbana, Illinois 61801, USA
*e-mail: bcunning@uiuc.edu

Colloidal quantum dots display a wide range of novel optical properties that could prove useful for many applications in photonics. Here, we report the enhancement of fluorescence emission from colloidal quantum dots on the surface of two-dimensional photonic crystal slabs. The enhancement is due to a combination of high-intensity near-fields and strong coherent scattering effects, which we attribute to leaky eigenmodes of the photonic crystal. By fabricating two-dimensional photonic crystal slabs that operate at visible wavelengths and engineering their leaky modes so that they overlap with the absorption and emission wavelengths of the quantum dots, we demonstrate that the fluorescence intensity can be enhanced by a factor of up to 108 compared with quantum dots on an unpatterned surface.

Colloidal quantum dots (QDs) are inorganic semiconductor crystals that typically have dimensions of a few nanometres[1–3]. In recent years, QDs have emerged as an important class of materials that promise to revolutionize many areas of nanotechnology. QDs derive their unique optical properties—such as a broad absorption spectrum, narrow, size-tunable emission spectrum, high photostability, quantum efficiency and strong nonlinear response—from quantum confinement effects. These attributes, coupled with the ability to functionalize QDs with organic molecules and render them compatible with other material systems, has made them important candidates for light sources[4–6], solar cells[7], optical switches[8] and fluorescent probes in sensitive biological assays[9,10]. Techniques that can more efficiently excite and extract the light emitted by QDs could therefore lead to improvements in high-brightness light sources, enhanced nonlinear response and lowering of the detection limits in biological assays.

Since their discovery by Wood[11] in 1902 and subsequent analysis[12–15], anomalies in periodically modulated structures have attracted much attention. Wang and Magnusson studied[16,17] resonant anomalies in waveguide gratings and showed that structures with a subwavelength modulation in refractive index along one dimension can function as filters that produce complete exchange of energy between forward- and backward-propagating diffracted waves with smooth line shapes and arbitrarily low linewidths[18]. This anomalous resonant phenomenon (termed guided-mode resonance) arises due to periodic index modulation, which allows phase-matching of

externally incident radiation into modes that can be re-radiated into free space. Due to the fact that these modes possess finite lifetimes within such structures, they are referred to as 'leaky eigenmodes' of the structures. More recently, guided-mode resonances have been studied and demonstrated in crossed gratings[19–21] or two-dimensional photonic crystal (PC) slabs[22–25]. The leaky nature of these modes has been successfully exploited towards the development of light-emitting diodes (LEDs) with improved extraction efficiency[26–28], biosensors[29] and vertically emitting lasers[30].

In this report, we study the interaction of QDs on the surface of a two-dimensional PC slab possessing leaky eigenmodes (hereafter referred to as leaky modes), spectrally overlapping both the absorption and emission spectra of the QDs. We demonstrate that the external excitation of the leaky modes leads to the formation of high-intensity near-fields that serve to efficiently excite the QDs. Additionally, the coupling of QDs to leaky modes overlapping their emission spectrum serves to enhance the QD emission preferred directions, by means of enhanced extraction. Such a doubly resonant scheme to enhance QD emission has not been demonstrated, until now.

ENHANCED EXCITATION AND EXTRACTION

When externally incident light interacts with periodically modulated structures in the subwavelength regime (as with PCs), only the zeroth-order forward- and backward-diffracted **Q1**
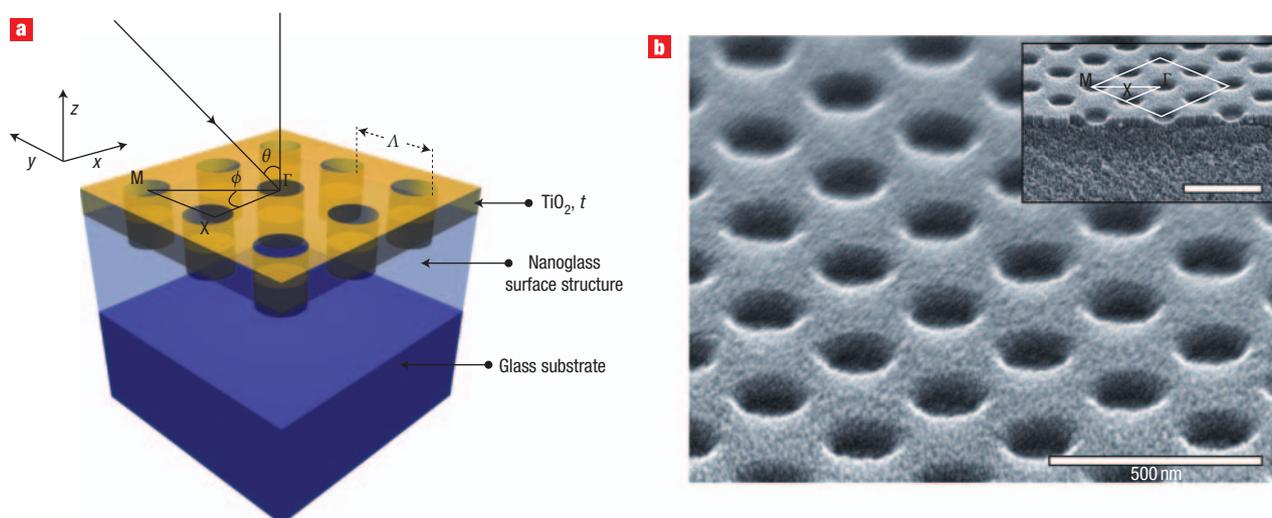
Figure 1 Visible-wavelength two-dimensional PC slab design and fabrication. **a**, Layout of the two-dimensional PC device. **b**, SEM images of a sample fabricated by the nanoreplica moulding approach. Γ, X and M are points of high symmetry. $\Lambda = 300$ nm is the period of the square lattice, $t = 125$ nm is the thickness of the high-index layer and θ is the angle the incident beam makes with the vertical. Scale bar = 500 nm.

waves can propagate. However, the periodicity also allows for phase-matching of higher (evanescent) orders to localized leaky modes supported by the PC. Once excited, the leaky modes, defined by a complex propagation constant, possess a finite lifetime as they are diffracted out both in the forward (transmitted) and backward (specular) directions. The backward re-radiated waves are in phase and constructively interfere with the zeroth backward-diffracted order, while the forward re-radiated waves are out of phase with the zeroth forward-diffracted order by π radians[31], causing destructive interference and consequently zero transmission. Thus, the external excitation of leaky modes is associated with a 100% reflection phenomenon for a resonant wavelength, assuming a defect-free, lossless system. As the excited leaky modes are localized in space during their finite lifetimes, they can be engineered to have very high energy density within regions of the PC at resonance. The magnitude of this energy density is directly related to the resonant mode lifetime or Q-factor of resonance, which in turn can be controlled by adjusting the device parameters. The intensity of emission of fluorescent species (which are absorptive at the resonant wavelengths) can be greatly enhanced by placing them in proximity to regions where the resonant modes concentrate most of their energy.

The existence of leaky modes overlapping the fluorescence emission spectrum opens up pathways for the emitted light to escape into free space. As well as direct emission, the fluorescence can now couple to the overlapping leaky modes and Bragg scatter out of the structure, thereby greatly reducing the amount of light trapped as guided modes, in comparison to an unpatterned substrate[27]. If the dispersion of these overlapping leaky modes is close to the Γ-point band-edge, that is, $K_{\parallel}$ (magnitude of the in-plane wave vector) ~ 0, most of the emitted light will be extracted within small angles to the surface normal. More generally, appropriately engineering the leaky dispersion of the PC facilitates the funnelling of guided light into regions of space where it can be easily detected. It can thus be appreciated that enhancement of fluorescence can be achieved in two steps: enhanced excitation and enhanced extraction.

PC DESIGN

In order to design a PC that could support multiple leaky modes, we chose a two-dimensional structure with a sufficiently large effective index and the features arranged as a square lattice of holes (Fig. 1a). The period (Λ) of the structure was chosen such that it supports high Q-factor resonant modes at a wavelength where the QDs are excited ($\lambda = 488$ nm, excitation mode) and low Q-factor modes overlapping the QD fluorescence emission spectrum (centred at $\lambda = 616$ nm, extraction mode). The logic governing the choice of low Q-factor extraction modes will become clear shortly. The depth of the holes was chosen to provide the required spectral separation between the excitation and extraction modes. The thickness t of the TiO$_2$ layer was chosen to fine-tune the spectral location of the resonant modes. The PC was cost-effectively fabricated by a nanoreplica moulding approach[32] and in an asymmetric configuration (the refractive index (RI) of the substrate was greater than that of the superstrate, air), so as to provide the required mechanical stability and maintain a simplistic fabrication procedure. A combination of high- and low-RI materials was important in order to provide sufficient effective index and positioning of the modes respectively. Using a low-RI substrate allows the modes to be positioned closer to the upper device surface, in contrast to a high-RI substrate, which would draw the modes deeper into the device and subsequently reduce their interaction with the QDs. Top surface and cross-section scanning electron microscopy (SEM) images of a fabricated device are shown in Fig. 1b.

RESULTS

Studying the reflection/transmission properties of PCs is a convenient technique to map out the dispersions of the leaky modes[25]. Rigorous coupled-wave analysis[33] (RCWA) simulations were used to simulate how the device would respond in transmission to externally incident illumination. Figure 2a shows the computed leaky mode band structure, which maps the spectral location and transmission efficiency of the resonances as a function of the launch angle, θ, along the Γ−M direction and
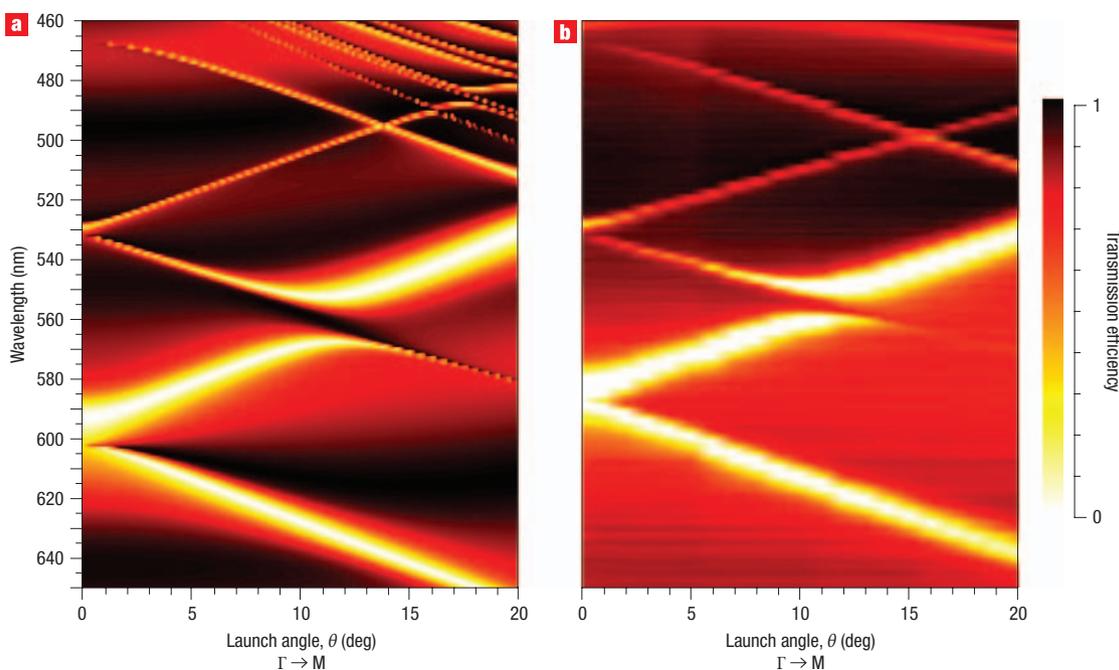
Figure 2 Leaky mode dispersion and efficiency. a,b, Calculated (**a**) and experimental (**b**) dispersion spectra of the fabricated PC device for white, S-polarized incident illumination incident along the $\Gamma - M$ direction. From both the theoretical and experimental dispersion it is seen that the leaky mode at $\lambda = 488$ nm is excited when the incident beam makes an angle $\theta = 11.2°$ with the surface normal. The excitation of the leaky mode at this wavelength, where the QDs are strongly absorbing, provides the required near-field enhancement for enhanced excitation. The colour scale shows the efficiency of transmission.

for S-polarized incidence. Experimental verification of the band structure of the fabricated device was carried out by mounting the device in a linear transmission setup, illuminating it with collimated white light and plotting the resulting transmitted spectrum as a function of θ (Fig. 2b). We see excellent agreement between simulation and experiment in the $460-500$ nm range, where the RIs of the materials do not change dramatically. Theoretically, we predict that the resonance at $\lambda = 488$ nm occurs at $\theta = 11.2°$, and this is accurately observed in experiment. At shorter wavelengths, the RI of TiO_2 begins to increase rapidly ($n_{TiO2} = 2.7$ at $\lambda = 400$ nm) and is considerably less at longer wavelengths ($n_{TiO2} = 2.36$ at $\lambda = 600$ nm), leading to deviations from simulations assuming a constant RI ($n_{TiO2} = 2.46$ at $\lambda = 488$ nm). This is clearly seen in the theoretically predicted higher-order bands originating from shorter wavelength resonances and redshifted longer wavelength bands, with which experimental results do not agree. For the excitation mode, the Q-factor of resonance was found to be 155.

Figure 3a,b shows the simulated electric field intensity (normalized to the unit amplitude incident field) at the two available surfaces of the device, for the excitation of the resonant mode at $\lambda = 488$ nm. The influence of the resonance phenomenon on the resulting near-fields is clearly seen as manifested in the enhanced electric field intensity. Similar enhancement can also be seen for the magnetic near-fields. It is apparent that for the lower available surface the excitation mode concentrates its energy within the cavity region (the term cavity is used here strictly in relation to the shape of the cross-section). At the upper surface, the energy is concentrated at the cavity periphery and beyond. Above the surfaces, the field intensity decays exponentially (as previously shown[34]) and practically with a finite QD size and unavoidable losses, the exact near-field intensity available to the QDs will always be lower than predicted. Nevertheless, studying the near-field intensity at the

available surfaces gives us a convenient metric to optimize the PC design. In our case, it is also important to mention that, due to the inherent asymmetry of the PC, the mode concentrates its energy in the high-index layer and is biased more towards the substrate. By reversing the asymmetry (by flooding the device surface with a higher-index material, such as water), we can reverse this biasing and to an extent draw the mode closer to the device surface, further increasing the mode interaction with the QDs. Such a modification will be easily adaptable for enhanced fluorescence biosensors, where the analytes are typically in an aqueous buffer solution. Near-field scanning optical microscopy (NSOM) images of the fabricated devices excited close to the resonant wavelength confirmed enhancement and spatial localization of the electric field (see Supplementary Information).

We now consider the effect of the leaky modes that overlap the emission spectrum of the QDs. In this enhanced extraction phenomenon, the Q-factor of the extraction modes will determine the rate at which coupled radiation will be scattered into free space. A low Q-factor (implying a short mode lifetime) would be beneficial in this case, as the coupled radiation can be scattered faster and thus the interaction of the radiation with losses in the system can be limited. A low Q-factor is also desirable from the standpoint that the radiation emitted from the QDs has a finite bandwidth, and a broad leaky resonance can scatter more of the emitted wavelengths in a given direction. Because the polarization and directions of the emitted fluorescence for a QD in free space can be assumed to be arbitrary, we consider the various available leaky modes that can interact with the emitted light. The experimentally determined dispersion of the leaky modes supported by the PC in the $\Gamma - X$ and $\Gamma - M$ directions and for orthogonal polarizations (S and P) is shown in Fig. 4. The case involving $\Gamma - M$ and S-polarization is already shown in Fig. 2b. It is clearly seen that the QD emission (centred at $\lambda = 616$ nm) can couple to leaky modes supported
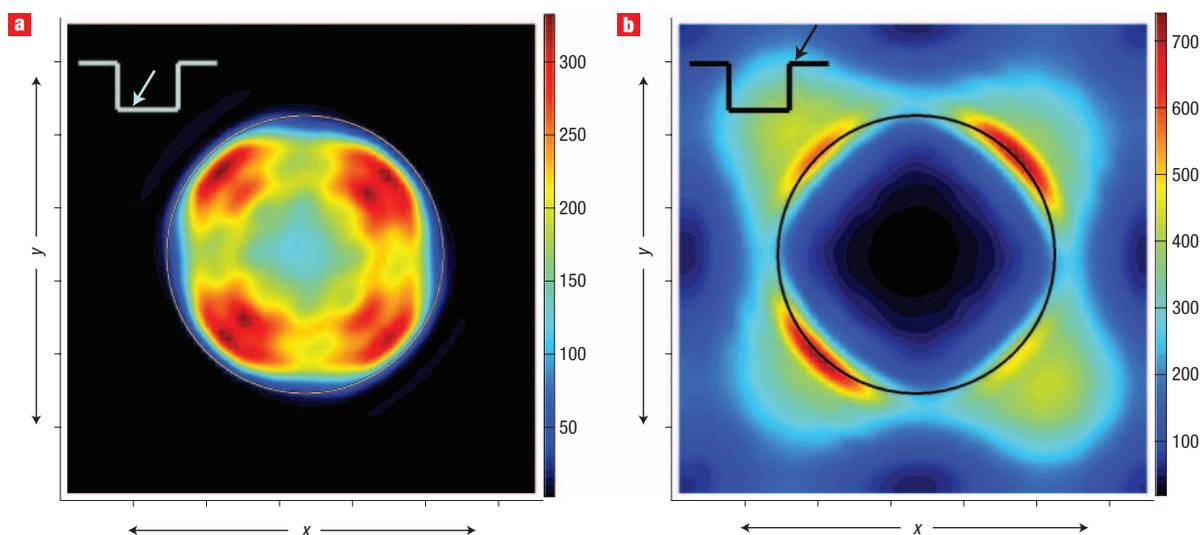
Figure 3 Near-field intensity calculations. a,b, Calculated near electric-field intensities (E^2) for the lower (**a**) and upper (**b**) device surfaces when the leaky mode (resonance) at $\lambda = 488$ is excited using S-polarized light making an angle $\theta = 11.2°$ with the surface normal, using RCWA. One period of the photonic-crystal lattice is shown, and periodic boundary conditions have been applied to the x and y extents. The intensity of the near-field is normalized to the unit amplitude incident wave.
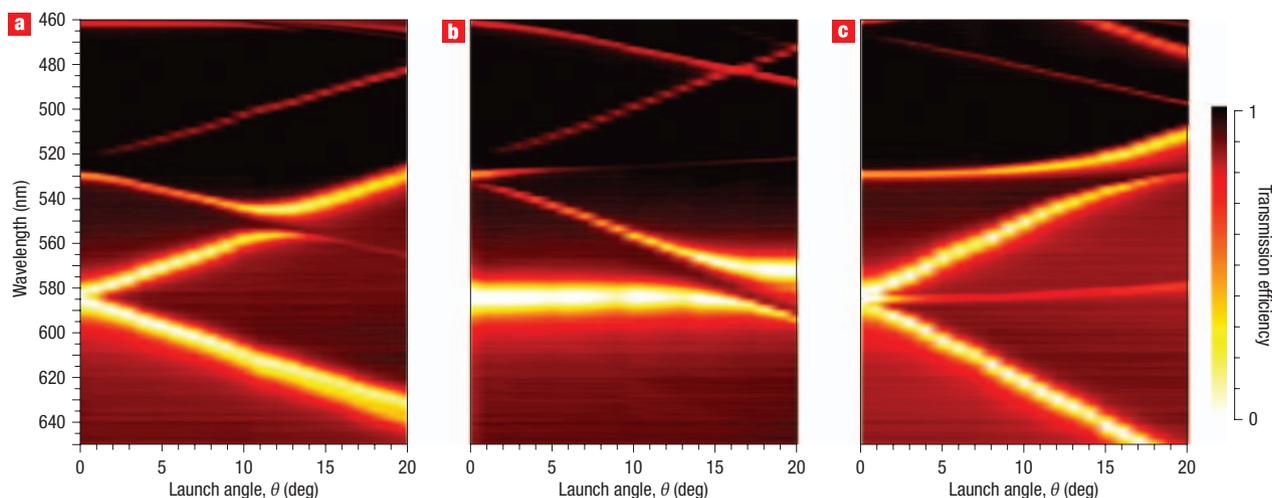

Figure 4 Leaky mode dispersion showing the possibility of enhanced extraction for all polarizations and directions of light. a–c, Experimentally determined dispersion spectra for the fabricated PC device probed with different polarizations and incident directions of white light: P-polarized and incident along the $\Gamma-M$ direction (**a**), P-polarized, $\Gamma-X$ (**b**) and S-polarized, $\Gamma-X$ (**c**).

by the PC and be extracted out of the device. From experiment, we find that the Q-factor for these extraction modes is 92.

To quantify the effects of the two fluorescence enhancement schemes, the fabricated devices were cleaned using deionized water/isopropyl alcohol, and the QDs (CdSe/ZnS core−shell type, Evident Technologies, peak emission at $\lambda = 616$ nm) were diluted in toluene and made up to a concentration of 1,235 nM. The dilute solution of QDs was drop-cast on and off (to serve as a reference) the PC surface. After drying of the spots, the devices were scanned on a commercially available laser scanner (LS 2000, Tecan), equipped with a 25-mW, 488-nm solid-state laser and a photo-multiplier tube (PMT) to record the fluorescence signals. The scanner provides the ability to launch the incident illumination at angles tunable from $0°$ to $25°$ in steps of $0.1°$, along a single vertical axis and single polarization. In order to

quantify the extraction and excitation enhancement effects, the devices were scanned at the resonant angle ($\theta = 11.2°$) and a non-resonant angle ($\theta = 0°$). For the sake of clarity, the resonant angle is defined as the launch angle, θ, for which the leaky mode at $\lambda = 488$ nm is excited. Figure 5a,b shows the scanned images taken at $\theta = 11.2°$ and $\theta = 0°$, respectively. The circular regions on the images show the areas over which intensity information was averaged. Table 1 shows the raw data measured in PMT counts for the two cases over multiple measurements.

For the resonant angle ($\theta = 11.2°$), the ratio of intensity as recorded on and off the PC (after subtracting the background) was 108.87 ± 4.09 times. When the PC was no longer resonant with the externally incident beam ($\theta = 0°$) the observed enhancement was lowered to 13.21 ± 0.26 times. We attribute this latter enhancement mainly to the enhanced extraction provided by the PC. As the
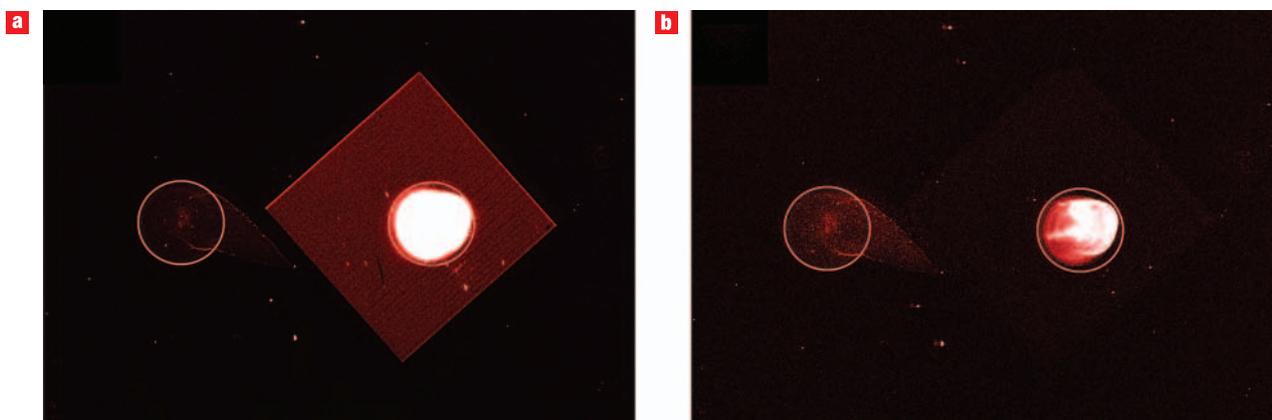
Q2

Figure 5 Enhanced fluorescence emission from QDs on the PC surface. Fluorescence (pseudocolour) scan images of the PC with QDs dispersed on the surface. **a**, Scan taken when the PC is resonant with respect to the incident beam ($\theta = 11.2°$), showing an enhancement factor of over 108 times. **b**, Scan taken when the PC is not resonant with the incident beam ($\theta = 0°$), showing an enhancement factor of over 13 times. The circular regions represent the area over which intensity information was averaged. In both images, the circle to the left shows the control region where no PC is present.

Table 1 Raw fluorescence signal, measured in PMT counts. The fluorescence intensity is measured from QDs on the PC both when it is in resonance and out of resonance with the incident beam. After subtracting the background in both cases, the enhancement due to the enhanced near-fields (enhanced excitation) and the enhancement due to coherent scattering (enhance extraction) are determined. Q5

	Signal		Background		Enhancement
	On PC (S_1)	Off PC (S_2)	On PC (B_1)	Off PC (B_2)	$(S_1 - B_1)/(S_2 - B_2)$
$\theta = 11.2°$	$10{,}160.93 \pm 362.92$	131.78 ± 2.91	336.03 ± 9.14	41.52 ± 1.13	108.89 ± 4.09
$\theta = 0°$	705.31 ± 8.80	72.52 ± 0.93	25.33 ± 0.89	21.04 ± 0.48	13.21 ± 0.26

extraction effect only relates to the dispersive properties of the PC, it should not be affected by a change in the launch angle of the incident light. Using this assumption, we divide the total enhancement obtained for the resonant angle by the enhancement obtained for the non-resonant angle and obtain a value of 8.24 ± 0.36 times for fluorescence enhancement by the near-fields.

DISCUSSION

At first glance, the result for fluorescence enhancement due to the enhanced near-fields is less than the peak intensity of the near-fields shown in Fig. 3a,b. However, one could expect that the spatially averaged near-field enhancement would be lower due to the specific pattern of the field distributions (see Supplementary Information), and more important in deciding the resulting enhancement due to the non-specific positioning of the QDs. Furthermore, we found that the inherent absorption and fluorescence at visible wavelengths of materials used in such fabrication processes results in additional loss to the resonance.

For the enhanced extraction case, the fluorescence enhancement is mostly related to Bragg scattering. The structure fabricated in this study, due to its asymmetric nature, cannot possess a bandgap for either transverse electric (TE)- or transverse magnetic (TM)-like modes and, therefore, the effect of inhibited spontaneous emission into undetectable waveguide modes is absent. We also performed time-resolved fluorescence measurements on the QDs both on and off the PC surface, which helped verify the absence of cavity-enhanced spontaneous emission through the Purcell effect[35] (data not shown). Enhanced extraction was also verified by angle-resolved fluorescence measurements. By illuminating the PC and measuring the

fluorescence emitted by the QDs at different angles, we were able to show strong coupling between the extraction modes and the QDs (see Supplementary Information). The extraction effects may be further optimized by reducing the anisotropy[36] of the in-plane wavevector, by using photonic lattices whose Brillouin zones are more circular, for example, the triangular or quasi-periodic lattices. The density of extraction modes will also affect the extraction efficiency. A greater density of modes that overlap the emission spectrum of the QDs would result in stronger scattering and consequently extraction effects. Finally, by engineering the spectral overlap and dispersion properties of the various leaky modes supported by the PCs, one can extend the enhancement effect to a wide range of fluorescent species.

Such a fluorescence enhancement scheme can be invaluable to the application of fluorescent biosensing using QDs. Given the excellent applicability of QDs to serve as fluorescent probes, we are developing a highly sensitive fluorescence detection system that will enable working at very low/single-molecule analyte concentrations. The detection scheme will inherently incorporate low background fluorescence, as the QD tags close to the biosensor surface will experience maximum fluorescence enhancement, similar to total internal reflection fluorescence[37] (TIRF) microscopy.

In conclusion, we have demonstrated resonant enhancement of over 108 times in fluorescence from QDs on the surface of a two-dimensional PC. This has been achieved by engineering the PC to possess leaky eigenmodes at the absorption and emission wavelengths of the QDs. We believe the results of this work can be adapted to realizing a wide variety of interesting optical applications involving QDs, including high-brightness LEDs, optical switches and high-sensitivity biosensors.

METHODS

FABRICATION

The two-dimensional PCs in this study were fabricated using nanoreplica moulding. Electron beam lithography (JEOL JBX-6000FS) was used to define a two-dimensional 'square lattice of holes' surface structure of period $\Lambda = 300$ nm and hole radius $r = 90$ nm on a SiO_2/Si substrate with PMMA as the mask layer. The pattern was exposed to a size of 3×3 mm^2 followed by development and dry-etching in a CHF_3 reactive-ion etching process. The resulting surface structure was subsequently transferred to a glass substrate, coated with a low-index porous spin-on-glass (Nanoglass, Honeywell) using an intermediate polydimethylsiloxane (PDMS) stamp. A thin layer of high-index TiO_2 ($t = 125$ nm) was then sputtered (AJA International) to form the final device. The RIs of the nanoglass and TiO_2 materials as determined by spectroscopic ellipsometry (Woolam) were $n_{NG} = 1.17$ and $n_{TiO2} = 2.46$ respectively at $\lambda = 488$ nm.

SIMULATION

A commercial implementation (DiffractMOD RSoft Design Group) of the RCWA code was used for all the simulations. One period of the device was simulated, with periodic boundary conditions applied to the x and y extents. The incident radiation was set to be S-polarized plane waves incident from above the device and along the $\Gamma - M$ direction ($\phi = 45°$; the choice of these launch parameters was essentially dictated by limitations of our experimental setup). To improve the calculation speed for the leaky-mode band structure, the materials were assumed lossless and the RI dispersion was assumed to be flat at about $\lambda = 488$ nm. Near-field calculations however, were performed including the complex component of the material refractive indices ($k_{NG} = 0$ and $k_{TiO2} = 0.00036$) and retaining 12 harmonics in both the x and y directions.

References

1. Henglein, A. Small-particle research: physicochemical properties of extremely small colloidal metal and semiconductor particles. *Chem. Rev.* **89,** 1861–1873 (1989).
2. Wilson, W. L., Szajowski, P. F. & Brus, L. E. Quantum confinement in size-selected, surface-oxidized silicon nanocrystals. *Science* **262,** 1242–1244 (1993).
3. Alivisatos, A. P. Semiconductor clusters, nanocrystals, and quantum dots. *Science* **271,** 933–937 (1996).
4. Colvin, V. L., Schlamp, M. C. & Alivisatos, A. P. Light-emitting-diodes made from cadmium selenide nanocrystals and a semiconducting polymer. *Nature* **370,** 354–357 (1994).
5. Coe, S., Woo, W.-K., Bawendi, M. & Bulovic, V. Electroluminescence from single monolayers of nanocrystals in molecular organic devices. *Nature* **420,** 800–803 (2002).
6. Bowers, M. J., McBride, J. R. & Rosenthal, S. J. White-light emission from magic-sized cadmium selenide nanocrystals. *J. Am. Chem. Soc.* **127,** 15378–15379 (2005).
7. Aroutiounian, V., Petrosyan, S., Khachatryan, A. & Touryan, K. Quantum dot solar cells. *J. Appl. Phys.* **89,** 2268–2271 (2001).
8. Nakamura, H. *et al.* Ultra-fast photonic crystal/quantum dot all-optical switch for future photonic networks. *Opt. Express* **12,** 6606–6614 (2004).
9. Chan, W. C. W. & Nie, S. Quantum dot bioconjugates for ultrasensitive nonisotopic detection. *Science* **281,** 2016–2018 (1998).
10. Alivisatos, P. The use of nanocrystals in biological detection. *Nat. Biotechnol.* **22,** 47–52 (2004).
11. Wood, R. W. On a remarkable case of uneven distribution of light in a diffraction grating spectrum. *Philos. Mag.* **4,** 392–402 (1902).
12. Rayleigh, L. On the dynamical theory of gratings. *Proc. R. Soc. Lond. Ser. A* **79,** 399–416 (1907).
13. Hessel, A. & Oliner, A. A. A new theory of Wood's anomalies on optical gratings. *Appl. Opt.* **4,** 1275–1297 (1965).
14. Popov, E., Mashev, L. & Maystre, D. Theoretical study of the anomalies of coated dielectric gratings. *Opt. Acta* **33,** 607619 (1986).
15. Bertoni, H. L., Cheo, L. H. S. & Tamir, T. Frequency selective reflection and transmission by a periodic dielectric layer. *IEEE Trans. Antennas Propag.* **37,** 78–83 (1989).
16. Wang, S. S., Magnusson, R. & Bagby, J. S. Guided-mode resonances in planar dielectric-layer diffraction gratings. *J. Opt. Soc. Am. A* **7,** 1470–1474 (1990).
17. Magnusson, R. & Wang, S. S. New principle for optical filters. *Appl. Phys. Lett.* **61,** 1022–1024 (1992).
18. Wang, S. S. & Magnusson, R. Theory and applications of guided-mode resonance filters. *Appl. Opt.* **32,** 2606–2613 (1993).
19. Peng, S. & Morris, G. M. Resonant scattering from two-dimensional gratings. *J. Opt. Soc. Am. A* **13,** 993–1005 (1996).
20. Peng, S. & Morris, G. M. Experimental demonstration of resonant anomalies in diffraction from two-dimensional gratings. *Opt. Lett.* **21,** 549–551 (1996).
21. Boonruang, S., Greenwell, A. & Moharam, M. G. Multiline two-dimensional guided-mode resonant filters. *Appl. Opt.* **45,** 5740–5747 (2006).
22. Suh, W. & Fan, S. All-pass transmission or flattop reflection filters using a single photonic crystal slab. *Appl. Phys. Lett.* **84,** 4905–4907 (2004).
23. Rosenberg, A. *et al.* Guided resonances in asymmetrical GaN photonic crystal slabs observed in the visible spectrum. *Opt. Express* **13,** 6564–6571 (2005).
24. Fan, S. & Joannopoulos, J. D. Analysis of guided resonances in photonic crystal slabs. *Phys. Rev. B* **65,** 235112 (2002).
25. Astratov, V. N. *et al.* Resonant coupling of near-infrared radiation to photonic band structure waveguides. *J. Lightwave Technol.* **17** (1999). **Q3**
26. Boroditsky, M. *et al.* Light extraction from optically pumped light-emitting diode by thin-slab photonic crystals. *Appl. Phys. Lett.* **75,** 1036–1038 (1999).
27. Boroditsky, M. *et al.* Spontaneous emission extraction and purcell enhancement from thin-film 2-D photonic crystals. *J. Lightwave Technol.* **17,** 2096–2112 (1999).
28. Erchak, A. A. *et al.* Enhanced coupling to vertical radiation using a two-dimensional photonic crystal in a semiconductor light-emitting diode. *Appl. Phys. Lett.* **78,** 563–565 (2001).
29. Cunningham, B. *et al.* A plastic colorimetric resonant optical biosensor for multiparallel detection of label-free biochemical interactions. *Sens. Act. B* **81,** 316–328 (2002).
30. Kobayashi, T., Kanamori, Y. & Hane, K. Surface laser emission from solid polymer dye in a guided mode resonant grating filter structure. *Appl. Phys. Lett.* **87,** 151106 (2005).
31. Rosenblatt, D., Sharon, A. & Friesem, A. A. Resonant grating waveguide structures. *IEEE J. Quant. Electron.* **33,** 2038–2059 (1997).
32. Ganesh, N., Block, I. D. & Cunningham, B. T. Near ultraviolet-wavelength photonic-crystal biosensor with enhanced surface-to-bulk sensitivity ratio. *Appl. Phys. Lett.* **89,** 023901 (2006).
33. Moharam, M. G. & Gaylord, T. K. Rigorous coupled-wave analysis of planar-grating diffraction. *J. Opt. Soc. Am.* **71,** 811–818 (1981).
34. Ding, Y. & Magnusson, R. Use of nondegenerate resonant leaky modes to fashion diverse optical spectra. *Opt. Express* **12,** 1885–1891 (2004).
35. Purcell, E. M. Spontaneous emission probabilities at radio frequencies. *Phys. Rev.* **69,** 681 (1946).
36. Ichikawa, H. & Baba, T. Efficiency enhancement in a light-emitting diode with a two-dimensional surface grating photonic crystal. *Appl. Phys. Lett.* **84,** 457–459 (2004).
37. Tamm, L. *Optical Microscopy: Emerging Methods and Applications* (Academic Press, New York, 1993).

Author contributions

Q4

Competing financial interests

PUBLISHER: Nature

PAPER NO.:   nnano.2007.216

AUTHORS: Nikhil Ganesh *et al.*

PAPER TITLE: Enhanced fluorescence emission from quantum dots on a photonic crystal surface

PAGE (AUTHOR'S MANUSCRIPT)	QUERY NO.	QUERY	RESPONSE
	1	"zeroth-order" OK as amended?	
	2	In Table 1, this value is given as 108.89, not 108.87 – please check.	
	3	Ref. 25, please provide page range	
	4	Authors are encouraged to include a statement called "Author contributions" to specify the contributions of each co-author, such as experimental work, project planning, data analysis, etc. The statement should be short, and refer to the authors by their initials.	
	5	Table 1 title – please spell out PMT.	